A&A 537, A28 (2012)
DOI: 10.1051/0004-6361/201117563

Astronomy & Astrophysics

The role of photospheric shearing motions in a filament eruption related to the 2010 April 3 coronal mass ejection

F. P. Zuccarello[1,2], P. Romano[2], F. Zuccarello[3], and S. Poedts[1]

[1] Centre for Plasma-Astrophysics, K.U. Leuven, Celestijnenlaan 200B, 3001 Leuven, Belgium
e-mail: francesco.zuccarello@wis.kuleuven.be
[2] INAF – Osservatorio Astrofisico di Catania, via S. Sofia 78, 95123 Catania, Italy
[3] Dipartimento di Fisica e Astronomia – Universitá di Catania, via S. Sofia 78, 95123 Catania, Italy

Received 24 June 2011 / Accepted 18 October 2011

ABSTRACT

Context. Coronal mass ejections (CMEs) are huge expulsion of solar plasma and magnetic field in the interplanetary medium. Understanding the physics that lies beyond the CME initiation is one of the most fascinating research questions. Several models have been proposed to explain the initiation of CMEs. However, which model better explains the different aspects of the initiation process and the early evolution of the CMEs is a subject of ongoing discussion.
Aims. We investigate the magnetic field evolution of NOAA 11059 in order to provide a further contribution to our understanding of the possible causes and mechanisms that lead to the initiation of the geoeffective CME that occurred on 2010 April 3.
Methods. Using KSO Hα images we determine the chirality of the active region and some properties of the filament that eventually erupted. Using SOHO/MDI line-of-sight magnetograms we investigate the magnetic configuration of NOAA 11059 by means of both linear force free and potential field extrapolations. We also determine the photospheric velocity maps using the Differential Affine Velocity Estimator (DAVE).
Results. We find that the magnetic configuration of the active region is unstable to the torus instability. Moreover, we find that persistent shearing motions characterized the negative polarity, resulting in a southward, almost parallel to the meridians, drift motion of the negative magnetic field concentrations.
Conclusions. We conclude that persistent and coherent shearing motions played a significant role in facilitating the eruption. These shearing motions increased the axial field of the filament eventually bringing the fluxrope axis to a height where the onset condition for the torus instability was satisfied. Our observations show that both the magnetic configuration of the system and the photopsheric dynamics that preceded the event, were favourable for the eruption to occur.

Key words. Sun: filaments, prominences – magnetic fields – Sun: activity

1. Introduction

Several models have been proposed to explain the initiation of coronal mass ejections (CMEs) (Forbes et al. 2006; Roussev & Sokolov 2006). Which model better explains the different aspects of the initiation process and the early evolution of the CMEs is a subject of ongoing discussion. However, it is clear that independently from the trigger mechanisms, the energy available for the eruption is stored in the current carrying magnetic fields that dominate the solar atmosphere. Even though a key element for an eruption to occur is the presence of currents, for example stored in twisted flux ropes, also the overlying field plays a key role in determining if a flux rope undergoes a full eruption or not (Török & Kliem 2005, 2007; Démoulin & Aulanier 2010). Kliem & Török (2006) proposed the torus instability as suitable mechanism for the initiation of CMEs. The torus instability occurs when the magnetic tension of the overlying (external) field drops faster then the hoop force of the flux rope embedded in this magnetic field. Recently, Guo et al. (2010) investigated a confined eruption that occurred on 2005 May 27 and found that the system was stable with respect to the torus instability. The magnetic tension of the overlying field can be reduced by, for example, cutting the tethers (Klimchuk 2001) of the overlying field by merging opposite polarities (Amari et al. 2000, 2003) or by the emergence of new magnetic flux (Chen & Shibata 2000). Another possible scenario that requires a more complex magnetic topology is the breakout model (Antiochos et al. 1999; MacNeice et al. 2004). In this scenario, the magnetic reconnection at the X-point will transfer magnetic field from the overlying magnetic flux system towards the side magnetic flux systems, eventually facilitating the eruption. The role that the mutual orientation between the overlying flux system and the flux rope field has in the amount of reconnected flux that is generated during the emergence processes, has been investigated numerically by Galsgaard et al. (2007). These authors found that when the flux systems are nearly anti-parallel, substantial reconnection is observed and the system also shows clear signatures of a high-temperature plasma located in the high-velocity outflow regions extending from the reconnection region. On the other hand, the cases that have a more parallel orientation of the flux systems show very limited reconnection and none of the associated features.

We study a filament eruption that occurred on 2010 April 3 in the active region NOAA 11059. The filament eruption resulted in the first geoeffective CME of the cycle 24. Wood et al. (2011) used a semi-empirical flux rope model in order to reproduce the event evolution in both COR1, COR2, HI1 and HI2 for both STEREO-A and STEREO-B spacecrafts and in SOHO/LASCO data. These authors concluded that based on the observations, it was not possible to unambiguously identify the relative position

between the axes of the flux rope model and the neutral line of the active region. This event has also been studied by Seaton et al. (2011) using observations from SWAP on board PROBA2 and SECCHI on board STEREO. The authors found that an initial flow of cold plasma in the low corona was observed prior to the eruption. They concluded that an initial mass off-loading process triggered a flux rope rise, but the eruption itself was due to the catastrophic loss of equilibrium of the flux rope. However, they could not address what caused the initial flow of mass from the active region.

In this paper we aim to investigate the role that the overlying magnetic field and the shearing motions played in the initiation of the 2010 April 3 CME. In particular, we focus our attention on the magnetic field, Hα and photospheric evolution of the active region. The structure of our paper is as follows. In Sect. 2 we present the data we use, while the data analysis and the results are presented in Sect. 3. Finally, in Sect. 4 we discuss the consequences of our results.

2. Observations

On 2010 April 3 at 09:05 UT in NOAA 11059 (S25 W03) a filament eruption occurred, resulting in a geoeffective CME. The GOES 14 satellite (Stern et al. 2004) recorded a B7.4 flare, beginning at 09:04 UT, with peak at 09:54 UT and ending at 10:58 UT, occurring in the same active region. The EUV evolution of the active region is presented in Seaton et al. (2011). According to these authors, at 08:18 UT a cold plasma blob was launched in the southward direction eventually destabilizing the filament that underwent a sudden expansion at around 08:55 UT.

In order to investigate the phenomenon that caused the launch of the cold plasma blob and the filament eruption, we studied the chromospheric evolution of the active region using Hα images of the filament taken at the Kanzelhöhe Observatory (KSO) on 2010 April 3 between 06:27 UT and 12:00 UT, having a spatial resolution of 2 arcsec and a time resolution of about 1 min. The coronal configuration of the active region was analyzed by means of SWAP data. SWAP (Berghmans et al. 2006; Halain et al. 2010) takes images at 174 Å, with a time resolution of about 100 seconds and a linear pixel size of about 3.17 arcsec. To analyze the magnetic configuration of NOAA 11059 we used the full-disk line-of-sight magnetograms taken by SOHO/MDI at 6767.8 Å with a spatial resolution of 3.96 arcsec and a temporal resolution of 96 min. We considered magnetograms acquired between 09:35 UT on 2010 April 2 and 09:35 UT on 2010 April 4 2010, i.e., from one day before the eruption up to one day after the eruption. We corrected all the magnetogram data for the angle between the magnetic field direction and the observer's line-of-sight. We considered subfields of 238×238 arcsec (120×120 pixels) centered on NOAA 11059 and aligned all subfields by applying a standard differential rotation rate (Howard et al. 1990) with a sampling of 1 arcsec, i.e., applying a subpixelization.

3. Data analysis and results

Figure 1a shows the KSO Hα image taken on 2010 April 3 at 07:33 UT. A filament crossing a facular region at the center of the field of view and extending along the north-south direction is visible. The filament presents a fragmented structure and is not clearly visible through the facular area. Just southward of the facula, a bifurcation is observed.

Figure 1b shows the SOHO/MDI magnetogram of the active region taken at 07:59 UT on 2010 April 3, while Fig. 1c shows

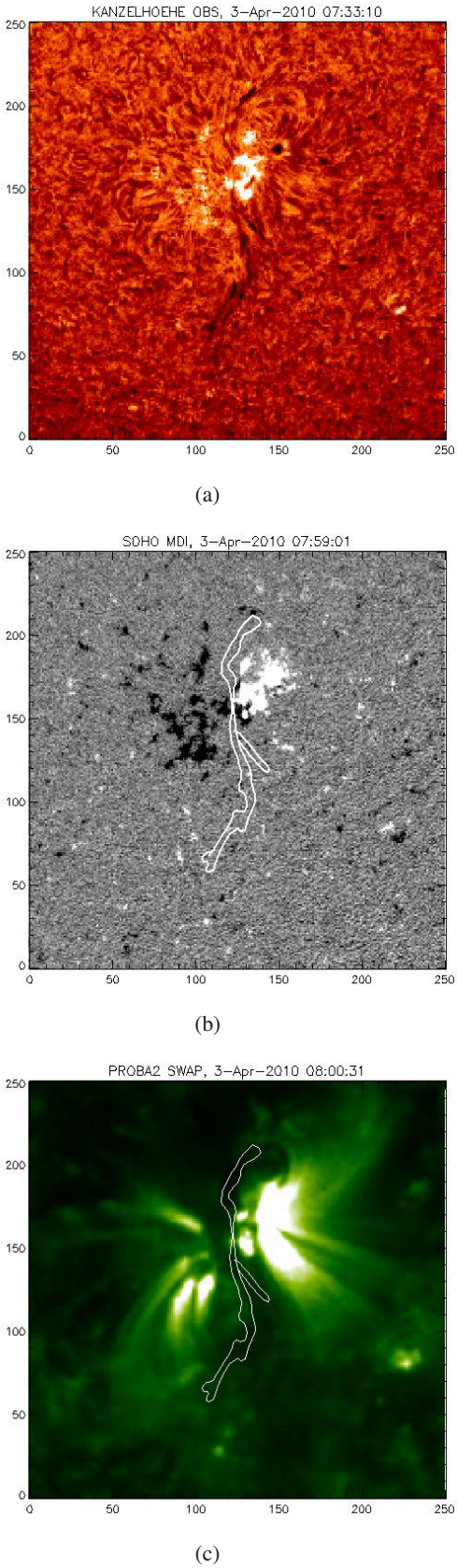

Fig. 1. Co-aligned images at different wavelengths and MDI magnetogram of the AR 11059. **a)** KSO Hα image of the filament; **b)** MDI magnetogram and **c)** SWAP EUV image taken at 174 Å. The white contour in the EUV and MDI images represents the boundaries of the Hα filament. Scale in the axis is the number of pixels. The field of view is $\sim 356 \times 356$ Mm^2. North is at the top and west to the right.

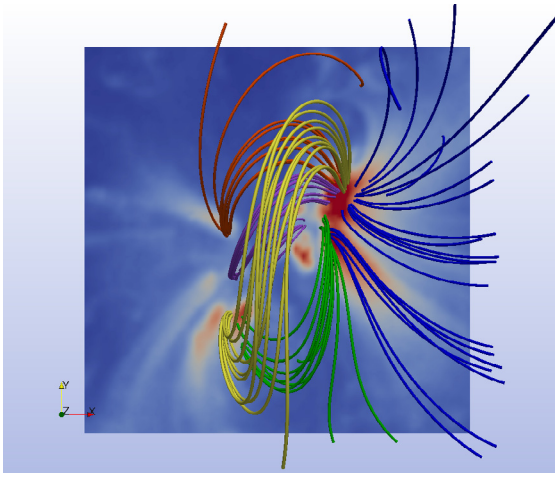

Fig. 2. Linear force-free field extrapolation for the MDI magnetogram taken on 2010 April 3 at 07:59 UT, superimposed on the SWAP image. Different colors indicate different field lines bundles (see text).

the 174 Å SWAP image taken on 2010 April 3 at 08:00 UT. We co-aligned the three images by using the SolarSoft routines. In particular, we first used the `index2map.pro` to create maps, i.e., IDL structures, from the fits files. Secondly, we applied the `map2earth.pro` routine to account for the fact that both the MDI magnetograms and the SWAP images were taken from space. Finally, we used the `coregmap.pro` to co-align the images taking into account the information provided in the headers.

In the Hα image we identified the contour of the filament and we over plotted it to the MDI magnetogram of the active region (Fig. 1b). The active region NOAA 11059 is characterized by a compact preceding positive polarity followed by a more fragmented negative polarity.

Figure 1c shows the EUV image of the active region together with the contour of the filament. The filament is fully included in the dark, forward-S shaped structure present in the EUV images. This gives us confidence that the fragmented filament visible in Hα is actually a single filament and not multiple filaments. The dark forward-S shape in the EUV image indicates that the active region presents a positive chirality (Canfield et al. 1999). This is also confirmed by the counter clockwise whirl around the preceding sunspot in the Hα image (Chae et al. 2001). In order to determine the sign of the magnetic helicity for the investigated active region, we performed a linear force free field extrapolation using the method introduced by Alissandrakis (1981). We found by visual inspection that the best agreement between the extrapolated field lines and the EUV images is obtained for the force free field parameter $\alpha = 0.02$. Figure 2 shows the result of this extrapolation overplotted to the SWAP image. Different colors represents field lines starting from different locations. Blue field lines are field lines starting from the edges of the positive polarity and that do not close within the extrapolation box. Green/violet/orange field lines are low lying magnetic arcades that connect the opposite polarities. The yellow field lines are closed field lines that extend higher in the solar corona, probably supporting and confining the filament.

In order to verify if the system was torus unstable, for the given magnetic field distribution, we calculated the decay index. The decay index n is defined as

$$n = -R\frac{\mathrm{d}}{\mathrm{d}R}\left(\ln B_{\mathrm{ex}}\right), \qquad (1)$$

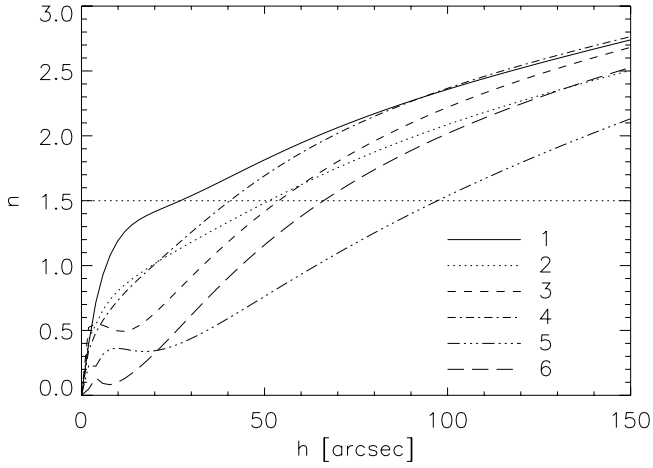

(a)

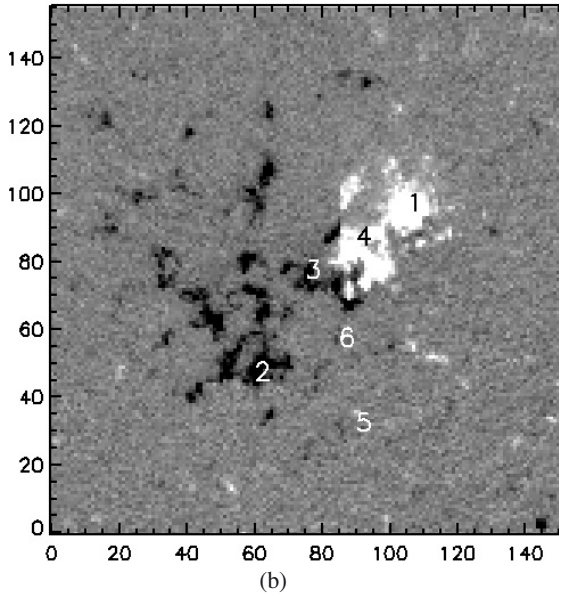

(b)

Fig. 3. a) Decay index for the potential field extrapolation as a function of the height above the photosphere. Different linestyles indicate different points in the active region; **b)** MDI magnetogram taken on 2010 April 3 at 07:59 UT. The numbers indicate selected points for which the decay index is shown.

where R is the flux rope major radius and B_{ex} is the external magnetic field. When n is larger than a critical value (n_{c}) the system becomes unstable. Démoulin & Aulanier (2010) found $n_{\mathrm{c}} \simeq 1.1$–$2$. To estimate the decay index from the observations some approximations have to be done. First we approximate the radius of the flux rope with the height from the photosphere (Török & Kliem 2007; Fan & Gibson 2007; Aulanier et al. 2010) and, second, we use the extrapolated potential field as a proxy of the external magnetic field (Guo et al. 2010). Figure 3a shows the decay index as a function of height for different locations above the photosphere. The points 3, 5 and 6 are taken along the filament (see Fig. 3b). Within an altitude of about 100 arcsec all the selected points have reached the critical value that is estimated as $\simeq$1.5. In particular, the central part of the filament (point 6) is more unstable to the torus instability with respect to the southern part of the filament (point 5).

In order to investigate the photospheric dynamics of the active region, we analyzed a sequence of MDI magnetograms.

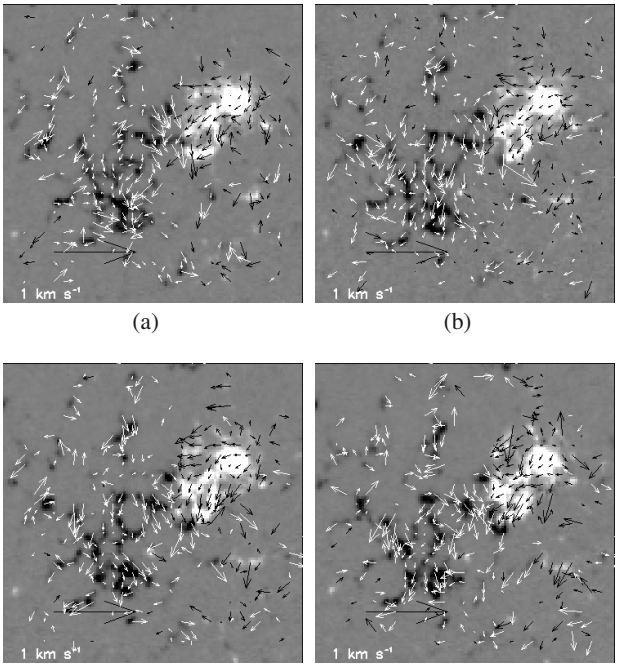

Fig. 4. Velocity field maps calculated using DAVE, by means of the magnetograms taken **a)** on 2010 April 2 between 12:51 UT and 14:27 UT; **b)** on 2010 April 2 between 17:36 UT and 19:15 UT; **c)** on 2010 April 2 between 20:51 UT and 22:27 UT; and **d)** on 2010 April 3 between 03:15 UT and 04:47 UT. The field of view is $\sim 171 \times 171$ Mm^2. North is at the top and west to the right.

More precisely, from the sequence of co-aligned MDI magnetograms, we determined the photospheric velocity maps using the Differential Affine Velocity Estimator (DAVE) (Schuck 2005). We used a full-width-at-half maximum of the apodization windows of 19.80 arcsec. Figure 4 shows some samples of these velocity maps. It is clear that persistent shearing motions characterize the fragmented negative polarity during the 24 h that preceded the eruption. These shearing motions are characterized by average velocities of 0.2–0.3 km s^{-1}. On the other hand, the larger positive polarity is characterized by definitely slower twisting motions. As a result of these motions, the negative flux concentrations moved southward by about 16–20 arcsec corresponding to 11–14 Mm, while the positive polarity mainly keeps its initial latitude. Furthermore, during the analyzed period, the total unsigned magnetic flux is of the order of 10^{22} Mx and shows variations not greater than 10 %, the steepest change actually occurring after the event.

In order to determine the connectivity of the magnetic field structures that characterized the active region on 2010 April 3 we performed a potential field extrapolation using the magnetograms taken at 09:35 UT on April 2 and at 07:59 UT on April 3 as boundary conditions. Figure 5 shows the results of these extrapolations for the magnetogram at 09:35 UT on April 2 (Figs. 4a, b)) and the one at 07:59 on April 3 (Figs. 4c, d)). The color scale in the side views is the longitudinal component of the magnetic field, while in the top views the field lines are overplotted to the high-contrasted Hα image. The different colors in the field lines represent different magnetic domains. Moreover, the same color in the field lines between the two magnetograms indicates field lines starting from the same magnetic flux distributions, i.e. the field lines are traced from those negative magnetic flux distributions, which evolution could have been followed in

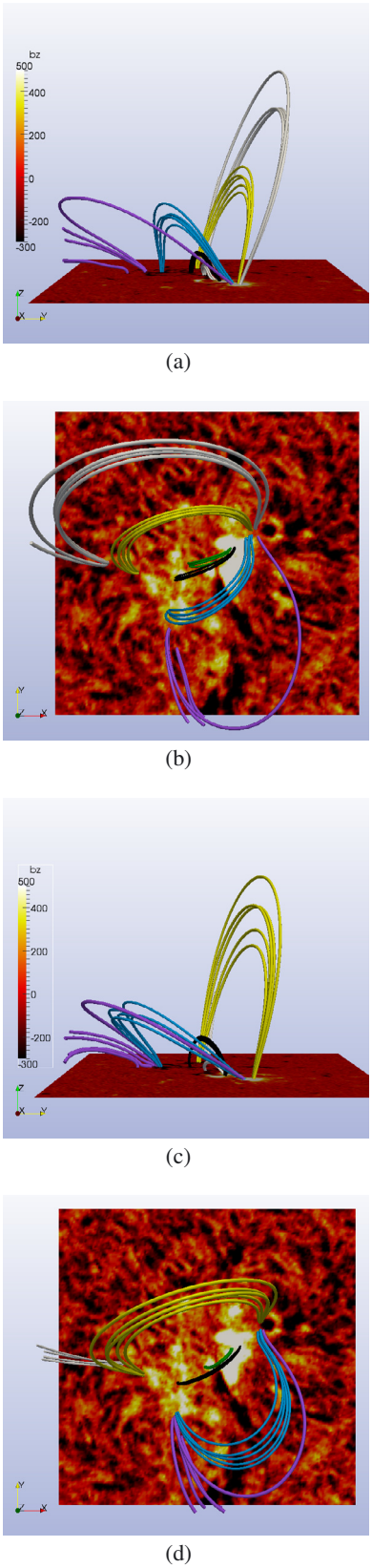

Fig. 5. Top and side views of the potential field extrapolations for the MDI magnetograms of the AR 11059 taken on 2010 April 2 at 09:35 UT **a)**, **b)** and on 2010 April 3 at 07:59 UT **c)**, **d)**, superimposed on the Hα images. In the side view, the red-white color scale is the magnetic field intensity. Different colors indicate different field lines bundles. Same colors between figures **a)**, **b)** and **c)**, **d)** indicate field lines starting from the corresponding flux distribution (see text).

the MDI sequence. Figure 5 confirms that the connectivity of the system did not change significantly during the analyzed period, i.e. no major flux emergence occurred for example in the proximity of the negative polarity, resulting in a different connectivity. Figures 5a and c show the side view of the extrapolated field for both magnetograms. Both the blue and violet field lines show an increase in their inclination, while from Figs. 5b and d a decrease in the angle between the axis of the filament and the green and black field lines is also visible. We registered a variation of the inclination angle between 4–10 degrees in about 24 h, with the bigger changes involving the field lines around the central part of the filament.

4. Discussion

In the previous section we used both H_α and EUV images to describe the morphology of the active region and of the filament that eventually erupted. We also used MDI magnetograms to investigate its magnetic evolution. Using the potential field extrapolations for the magnetogram at the moment of the eruption we calculated the decay index for the torus instability. It is interesting that among all the selected regions the most stable is the one corresponding to the southern part of the filament, that according to Seaton et al. (2011) is the one that resulted in the initial mass flow. Moreover, from their three-dimensional reconstructions the authors found that the initial altitude of a loop, presumably resembling the top of the fluxrope, was about 120 Mm. If we assume that the fluxrope fills all the space between the photosphere and its top, its axis has an altitude of about 60 Mm, i.e. about 83 arcsec. From Fig. 3a it is evident that five out of six curves have already reached the critical value 3/2 for the decay index indicating that, within the approximation errors, the system was torus unstable.

During the 24 h that preceded the eruption, the negative polarity of the active region was subjected to persistent and coherent southwards directed shearing motions. These shearing motions may have played a significant role in the eruption. In fact, even though the system was nominally torus unstable, the filament was observed for at least two days before the eruption. Therefore, other effects that are not taken into account in the estimation of the decay index, such as the line tying (Olmedo & Zhang 2010) and a non-zero toroidal component of the ambient field, may have played a role in stabilizing the filament. However, the observed shearing motions may have contributed to reduce these stabilising effects and they also resulted in the increase of the axial flux of the filament and as a consequence in the increase of its magnetic pressure. This increase in the magnetic pressure lifted up the flux rope slowly, eventually bringing its axis to a height where the condition for the torus instability is satisfied, resulting in the filament eruption.

Finally, the potential field extrapolations also show a decrease of the angle between the overlying field and the filament axis. According to Galsgaard et al. (2007) this should result in a decrease in the efficiency of the magnetic reconnection between the overlying field and ambient field, eventually stabilising the system. Nevertheless the filament erupted. This is a further evidence that for this event the torus instability may have played a significant role in triggering the eruption.

In conclusion, our observations show that both the magnetic configuration of the system and the photopsheric dynamics that preceded the event resulted in a configuration that was favourable for the eruption to occur.

Acknowledgements. The authors wish to thank the referee, whose comments and suggestions led to a significant improvement of the paper. These results were obtained in the framework of the projects GOA/2009-009 (K.U. Leuven), G.0729.11 (FWO-Vlaanderen), and C 90347 (ESA Prodex 9). Financial support by the European Commission through the SOLAIRE Network (MTRN-CT-2006-035484) is gratefully acknowledged. We gratefully acknowledged the Kanzelhhe Solar Observatory for providing the H_α images. SWAP is a project of the Centre Spatial de Liege and the Royal Observatory of Belgium funded by the Belgian Federal Science Policy Office (BELSPO).

References

Alissandrakis, C. E. 1981, A&A, 100, 197
Amari, T., Luciani, J. F., Mikić, Z., & Linker, J. A. 2000, ApJ, 529, L49
Amari, T., Luciani, J. F., Aly, J. J., Mikić, Z., & Linker, J. A. 2003, ApJ, 585, 1073
Antiochos, S., DeVore, C., & Klimchuk, J. 1999, ApJ, 510, 485
Aulanier, G., Török, T., Démoulin, P., & DeLuca, E. E. 2010, ApJ, 708, 314
Berghmans, D., Hochedez, J. F., Defise, J. M., et al. 2006, Adv. Space Res., 38, 1807
Canfield, R. C., Hudson, H. S., & McKenzie, D. E. 1999, Geophys. Res. Lett., 26, 627
Chae, J., Wang, H., Qiu, J., et al. 2001, ApJ, 560, 476
Chen, P., & Shibata, K. 2000, ApJ, 545, 524
Démoulin, P., & Aulanier, G. 2010, ApJ, 718, 1388
Fan, Y., & Gibson, S. E. 2007, ApJ, 668, 1232
Forbes, T. G., Linker, J. A., Chen, J., et al. 2006, Space Sci. Rev., 123, 251
Galsgaard, K., Archontis, V., Moreno-Insertis, F., & Hood, A. W. 2007, ApJ, 666, 516
Guo, Y., Ding, M. D., Schmieder, B., et al. 2010, ApJ, 725, L38
Halain, J.-P., Berghmans, D., Defise, J.-M., et al. 2010, in SPIE Conf. Ser., 7732
Howard, R. F., Harvey, J. W., & Forgach, S. 1990, Sol. Phys., 130, 295
Kliem, B., & Török, T. 2006, Phys. Rev. Lett., 96, 255002
Klimchuk, J. A. 2001, in Space Weather, ed. P. Song, H. J. Singer, & G. L. Siscoe (AGU), Geophys. Monograph Series, 125, 143
MacNeice, P., Antiochos, S. K., Phillips, A., et al. 2004, ApJ, 614, 1028
Olmedo, O., & Zhang, J. 2010, ApJ, 718, 433
Roussev, I. I., & Sokolov, I. V. 2006, in Solar Eruptions and Energetic Particles, ed. N. Gopalswamy, R. Mewaldt, & J. Torsti (AGU), Geophys. Monograph Series, 165, 89
Schuck, P. W. 2005, ApJ, 632, L53
Seaton, D. B., Mierla, M., Berghmans, D., Zhukov, A. N., & Dolla, L. 2011, ApJ, 727, L10
Stern, R. A., Shing, L., Catura, P. R., et al. 2004, in SPIE Conf., Ser. 5171, ed. S. Fineschi, & M. A. Gummin, 77
Török, T., & Kliem, B. 2005, ApJ, 630, L97
Török, T., & Kliem, B. 2007, Astron. Nachr., 328, 743
Wood, B. E., Wu, C.-C., Howard, R. A., Socker, D. G., & Rouillard, A. P. 2011, ApJ, 729, 70